Top-emitting white organic light-emitting devices with a one-dimensional metallic–dielectric photonic crystal anode

Wenyu Ji,[1,2] Letian Zhang,[1] Tianyu Zhang,[1] Guoqiang Liu,[2] Wenfa Xie,[1,*] Shiyong Liu,[1] Hanzhuang Zhang,[2,4] Liying Zhang,[3] and Bin Li[3]

[1]*State Key Laboratory on Integrated Optoelectronics, College of Electronic Science and Engineering, Jilin University, Changchun 130012, China*

[2]*Department of Physics, Jilin University, Changchun 130023, China*

[3]*Key Laboratory of Excited State Processes, Changchun Institute of Optics, Fine Mechanics and Physics, Chinese Academy of Sciences, Changchun 130033, China*

[4]*hzzhang@mail.jlu.edu.cn*

**Corresponding author: xiewf@jlu.edu.cn*

Received April 27, 2009; revised July 30, 2009; accepted August 3, 2009; posted August 17, 2009 (Doc. ID 110602); published September 4, 2009

Top-emitting white organic light-emitting devices (TEWOLEDs) with 1D metallic–dielectric photonic crystal (1D MDPC) as an anode are investigated. A quasi-periodic 1D MDPC anode allowed for fabrication of multiple-peak TEWOLEDs. A two-peak or three-peak TEWOLED was obtained by simply adjusting the thickness of the dielectric layers in the MDPC. The efficiency of the TEWOLEDs are comparable to the corresponding bottom WOLED (11.1 cd/A), which are 9.9 (two-peak device) and 9.4 cd/A (three-peak device), respectively, and the contrast of the TEWOLEDs is about twice as high as the bottom device owing to the low reflection of the anode.

OCIS codes: 230.3670, 050.2230, 240.0310.

A white organic light-emitting device (WOLED) is of interest owing to its potential application in flat-panel displays and illumination. Top-emitting WOLEDs (TEWOLEDs) with red, green, and blue color filters could provide a high-aperture ratio and a high resolution in active-matrix OLEDs. Besides, the currently used rather expensive glass substrates coated with indium tin oxide (ITO) are a disadvantage of the usual bottom-emitting OLEDs, especially for the large-area illumination devices. TEWOLEDs will be superior to bottom ones, because they can fabricate on opaque and flexible substrates, such as metal foils. However, owing to the strong microcavity effect, it remains a challenge to generate white light in a top-emitting device. Thus extensive efforts have focused on eliminating the microcavity effects in TEWOLEDs [1–3]. Besides, the TEWOLED utilizing the microcavity effect [4] and a TEWOLED with downconversion phosphors were reported [5]. However, there are some disadvantages of the reported TEWOLED. For example, the contrast is low in the TEWOLED with a high reflection anode and a high transmission cathode, and the efficiency is low in the TEWOLED utilizing the microcavity effect.

A three-peak, bottom-emitting, WOLED with thin metal/dielectric/thin metal/dielectric/thick metal as a cathode was reported [6] and gives much enhanced color gamut for full-color OLED display. In this Letter, we report the TEWOLEDs utilizing a quasi-periodic 1D metallic–dielectric photonic crystal (1D MDPC) as an anode. A two-peak or three-peak TEWOLED was obtained by simply adjusting the thickness of the dielectric layers in the MDPC.

The resonant wavelength (RW) condition of the microcavity for normal incidence is determined by the Fabry–Perot peak condition [7],

$$\sum_i \frac{4\pi d_i n_i(\lambda)}{\lambda} - \phi_{\mathrm{cathode}}(0,\lambda) - \phi_{\mathrm{anode}}(0,\lambda) = 2m\pi,$$

where λ is the emission wavelength; $\phi_{\mathrm{cathode}}(0,\lambda)$ and $\phi_{\mathrm{anode}}(0,\lambda)$ are the angle- and the wavelength-dependent phase changes on reflection from top cathode and bottom anode, respectively; m is an integer that defines the mode number; and $n_i(\lambda)$ and d_i are the refractive index and thickness of the organic layers.

Top-emitting devices with a structure of silica-coated silicon substrate/anode/MoO_x (1.5 nm)/4,4′,4″-tris(3-methylphenyl-phenylamino)-tripheny-lamine (m-MTDATA, 28 nm)/*N*,*N*′-bis-(1-naphthyl)-*N*,*N*′ diphenyl-1,1-biphenyl-4,4′diamine (NPB, 10 nm)/4,4′-bis(2,2′-diphenylvinyl)-1,1′-biphenyl (DPVBi, 15 nm)/4,4-*N*,*N*-dicarbazole-biphenyl (CBP, 5 nm)/CBP:bis(2-(2-fluorphenyl)-1,3-benzothiozolato-N,C2′) iridium(acetylacetonate) [$(F\text{-}BT)_2Ir(acac)$] (7 nm)/4,7-diphenyl-1,10-phenanthroline (Bphen, 30 nm)/LiF (1 nm)/Al (1 nm)/Ag (20 nm)/MoO_x (35 nm) were fabricated. In the devices, 1.5 nm MoO_x, m-MTDATA, NPB, DPVBi, CBP:$(F\text{-}BT)_2Ir(acac)$, Bphen, LiF/Al/Ag and 35 nm MoO_x were used as the buffer layer, the hole-injection layer, the hole-transporting layer, the blue-emitting layer, the orange-emitting layer, the electron-transporting layer, the cathode, and the light-outcoupling layer, respectively. The neat CBP is introduced to separate blue and organic emitting layers. Detailed processes of fabrication and measurement for OLEDs have been described in a previous paper [5].

Two anodes were built in experiment by carefully designing layer thicknesses, anode 1 for device A: Ag (150 nm)/tris-(8-hydroxyquinoline) aluminum (Alq_3, 75 nm)/Ag(20 nm)/Alq_3 (45 nm)/Ag (20 nm), anode 2 for device B: Ag (150 nm)/Alq_3 (95 nm)/Ag(20 nm)/Alq_3 (85 nm)/Ag (20 nm). For comparison, the bottom-emitting device (ITO glass substrate) with the same organic layers (device C) was fabricated. Figure 1 (top) shows the calculated round-trip phase changes for 95 nm organic layers sandwiched between two reflection electrodes [i.e., $\phi_1(\lambda)=\Sigma_i 4\pi d_i n_i(\lambda)/\lambda$], and the phase changes at two reflective electrodes [i.e., $\phi_2(\lambda)=\phi_{\mathrm{cathode}}+\phi_{\mathrm{anode}}$, incidence media are Bphen and m-MTDATA for cathode and anode, respectively]. The points of the intersection of $\phi_1(\lambda)$ and $\phi_2(\lambda)$ are the RWs of the device. Alq_3 is used as the dielectric material owing to its high transparency in the visible range and its compatibility with the OLED fabrication [8]. Ag is used as the metal owing to its lower absorption loss in the visible range and the highest conductivity among electrode materials. The phase shift is calculated by the transfer-matrix method [9]. It can be seen that two RWs at blue (465 nm) and yellow (549 nm) or three RWs at blue (436 nm), green (514 nm), and red (599 nm) will occur in the designed devices.

The normalized measured electroluminescence (EL) spectra at voltage of 9 V and the viewing angle of 0° for devices A, B, and C are shown in Fig. 1 (bottom). The spectrum of device C shows two main peaks at 448 and 548 nm originating from DPVBi and $(F\text{-}BT)_2Ir(acac)$, and the spectrum of device A shows two resonant emission peaks at 468 and 548 nm, while that of device B shows three resonant emission peaks at 436, 500, and 584 nm. The emission peaks of devices A and B are in excellent agreement with calculated results, and the RWs of device A are near the DPVBi and $(F\text{-}BT)_2Ir(acac)$ emission peaks, which will benefit the efficiency enhancement. We can also see that the narrowness of the FWHM of the DPVBi and $(F\text{-}BT)_2Ir(acac)$ emission in device A is observed. These results indicated that strong microcavity effect occurred in the top-emitting devices.

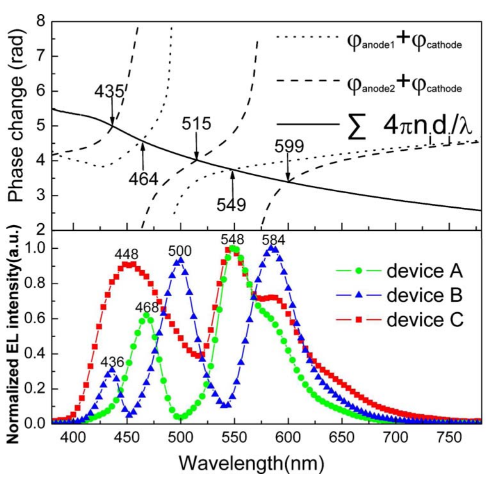

Fig. 1. (Color online) Calculated round-trip phase changes for 95 nm organic layers between two electrodes and the phase changes on two electrodes, and the normalized measured EL spectra of the white devices.

Figure 2 shows the normalized EL spectra and Commission Internationale de L'Eclairage coordinates of device A at different viewing angles and a voltage of 9 V. With increasing viewing angle, the peak wavelength shifts to a shorter wavelength, owing to the microcavity effect in the device, and a warm white emission with a CIE coordinate of (0.351, 0.422) at a viewing angle of 0° was obtained and changed to (0.323, 0.415) at 30° and (0.292, 0.411) at 60°. The CIE coordinates are fairly stable over a range of operation voltages. At a viewing angle of 0°, the CIE coordinates change from (0.343, 0.411) at 6 V to (0.351, 0.423) at 8 V then to (0.345, 0.414) at 11 V. The same characteristic is also observed at viewing angles of 30° and 60°.

A two-peak white device could be used as illumination, but it is not suitable for displays. Thus, a three-peak device (device B) is designed in our experiment. Figure 3 shows the normalized EL spectra of the device at a different viewing angle and a voltage of 9 V; the inset is the normalized EL spectra at a different voltage and a viewing angle of 0°. The blueshift of the peak wavelength with increasing viewing angle is also observed in this device. A white emission with a CIE coordinates of (0.429, 0.421) at viewing angle of 0° was obtained, and the CIE coordinates change to (0.404, 0.425) at 30° and (0.328, 0.394) at 60°, which are within the white region. As the bias increases, the blue and green emissions increase. The CIE coordinates change from (0.472, 0.437) to (0.395, 0.408) over a range of operation voltages from 6 to 11 V.

Figure 4 shows the voltage-current density-luminance and efficiency-voltage characteristics of the devices. It can be seen that device C exhibits a lower current density than devices A and B. We attributed this to the efficient hole injection from the Ag/MoO_x layer [10]. The luminance of devices A, B, and C are 16950, 12900, and 8960 cd/m^2 at 10 V, respectively, and the efficiencies of the TEWOLEDs are comparable to the bottom device. The maximum current efficiency of the devices are 9.9, 9.4, and 11.1 cd/A for devices A, B, and C, respectively. The reduction in current efficiency of the TEWOLED can be attributed to the low-reflection of the anode, as shown in Fig. 5.

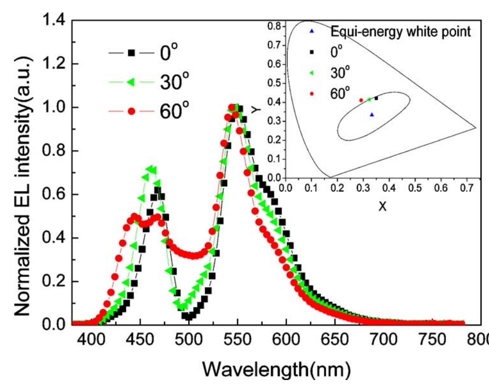

Fig. 2. (Color online) Normalized measured EL spectra of device A at different viewing angles and voltage of 9 V. Inset, CIE coordinate of device A at different viewing angles.

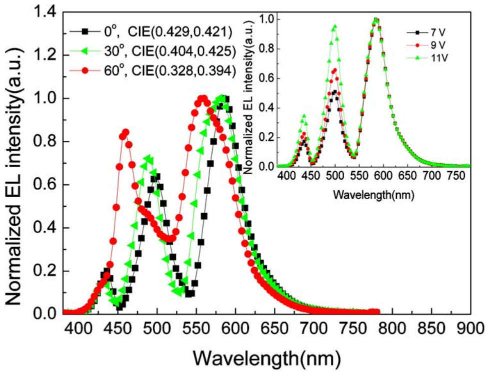

Fig. 3. (Color online) Normalized measured EL spectra of device B at different viewing angles and voltage of 9 V. Inset, normalized measured EL spectra of device B at different voltages.

The pixel contrast ratio (PCR) of devices is investigated as depicted in [11,12]. The light source D65 is utilized for calculation. In the calculation, the brightness of the devices at on- and off-state is set to be 1000 and 0 cd/m^2. The PCRs of devices A and B are 52:1 and 77:1 under an ambient illumination of 140 lx, corresponding to an enhancement of 86 and 175% over that of device C. The obvious improvement of PCR in devices A and B originates from the reduction of the reflectance in the whole visible region (Fig. 5), and the 1-D MDPC anode plays an important role in the absorption of ambient light. The 1-D MDPC effectively reduces the reflection of ambient light, as can be seen from Fig. 5.

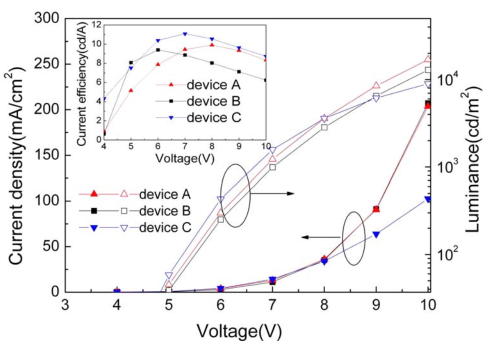

Fig. 4. (Color online) Voltage-current density-luminance and efficiency-voltage characteristics of the white devices.

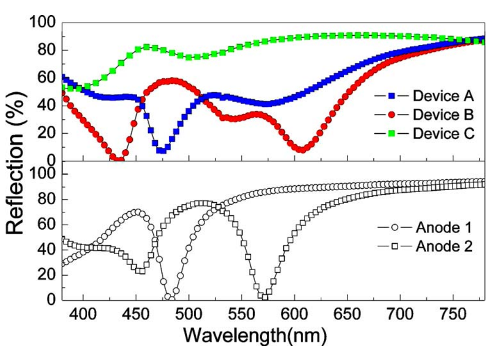

Fig. 5. (Color online) Reflection of the anodes and the white devices.

In summary, TEWOLEDs with a quasi-periodic 1D MDPC anode are demonstrated. Two-peak or three-peak white devices are obtained by simply adjusting the thickness of the dielectric layer in the MDPC. In principle, a multiple-peak TEWOLED with EL peaks at desired wavelengths can be achieved by adjusting the thickness of the dielectric–metal layer or the period of the MDPC, and the efficiency of the TEWOLEDs is comparable with the corresponding bottom device, while the contrast of the TEWOLED is higher than that of the bottom one. This result provides a guidance in the fabrication of TEWOLED with optimum performance, such as efficiency and color purity.

This work was supported by the National Natural Science Foundation of China (NSFC) (grants 60606017, 60707016, 60723002, and 10774060), the National High Technology Research and Development Program of China (grant 2006AA03A162), the Ministry of Science and Technology of China (grant 2010CB327701), and the Graduate Innovation Fund of Jilin University (grant 20091007).

References

1. H. Kanno, Y. R. Sun, and S. R. Forrest, Appl. Phys. Lett. **86**, 263502 (2005).
2. S. F. Hsu, C. C. Lee, S. W. Hwang, and C. H. Chen, Appl. Phys. Lett. **86**, 253508 (2005).
3. M. T. Lee and M. R. Tseng, Curr. Appl. Phys. **8**, 616 (2008).
4. M. S. Kim, C. H. Jeong, J. T. Lim, and G. Y. Yeom, Thin Solid Films **11**, 3590 (2008).
5. W. Y. Ji, L. T. Zhang, R. X. Gao, L. M. Zhang, W. F. Xie, H. Z. Zhang, and B. Li, Opt. Express **16**, 15489 (2008).
6. Y. J. Lu, C. H. Chang, C. L. Lin, C. C. Wu, H. L. Hsu, L. J. Chen, Y. T. Lin, and R. Nishikawa, Appl. Phys. Lett. **92**, 123303 (2008).
7. A. B. Djurišić and A. D. Rakić, Appl. Opt. **41**, 7650 (2002).
8. C. L. Lin, H. C. Chang, K. C. Tien, and C. C. Wu, Appl. Phys. Lett. **90**, 071111 (2007).
9. C. L. Mitsas and D. I. Siapkas, Appl. Opt. **34**, 1678 (1995).
10. J. Cao, X. Y. Jiang, and Z. L. Zhang, Appl. Phys. Lett. **89**, 252108 (2006).
11. J. A. Dobrowolski, B. T. Sullivan, and R. C. Bajcar, Appl. Opt. **31**, 5988 (1992).
12. Z. Y. Xie and L. S. Hung, Appl. Phys. Lett. **84**, 1207 (2004).